Journal of Alloys and Compounds 673 (2016) 327–335

Contents lists available at ScienceDirect

Journal of Alloys and Compounds

journal homepage: http://www.elsevier.com/locate/jalcom

Plastic deformation behavior of a thermo-mechanically processed AZ31 magnesium alloy under a wide range of temperature and strain rate

Farhoud Kabirian [a, *], Akhtar S. Khan [a], Thomas Gnäupel-Herlod [b]

[a] Department of Mechanical Engineering, University of Maryland, Baltimore County, Baltimore, MD 21250, USA
[b] NIST Center for Neutron Research, Gaithersburg, MD 20899-8562, USA

ARTICLE INFO

Article history:
Received 26 December 2015
Received in revised form
14 February 2016
Accepted 16 February 2016
Available online 19 February 2016

Keywords:
Twinning
Texture
Anisotropic material
Mechanical testing

ABSTRACT

Effects of texture evolution and grain refinement induced by Equal Channel Angular Pressing, ECAP, on mechanical responses of an extruded AZ31 magnesium alloy are investigated. Uniaxial compression loading is carried out under a wide range of temperature (77 K–423 K) and strain rate (10^{-4} s^{-1} –3000 s^{-1}) along pressing direction (PD), transverse direction (TD), and normal direction (ND). The s-shape strain hardening curve which is the main characteristic of twin-dominated deformation shows a strong dependency on testing temperature and strain rate in the ECAPed material so that during loading at the highest temperature (423 K) and the lowest strain rate (10^{-4} s^{-1}), s-shape hardening is no longer present. However, measured texture under the mentioned loading condition reveals crystal reorientation due to twinning which implies that the absence of concaved-up stress–strain curve is not necessarily indicative of suppression of twinning. On the other hand, the measured texture during high temperature dynamic loading suggests saturation of twinning at smaller strains. Schmid factor maps, in agreement with Visco-Plastic Self Consistent (VPSC) models, suggest the higher activity of twinning and basal slip in plastic yielding of the extruded and ECAPed AZ31, respectively.

1. Introduction

The great interest for weight reduction paid by the transportation industry has made magnesium alloys a center of attention. However, development of magnesium alloys for this purpose is confronted by many challenges such as low corrosion resistance, unacceptable mechanical properties at high temperatures, and poor ductility. It is known that an insufficient number of slip systems in magnesium alloys results in poor ductility. In order to improve this deficiency, special attention has been dedicated to producing ultra-fine grain magnesium through severe plastic deformation (SPD), in particular Equal Channel Angular Pressing, ECAP [1–6]. In general, depending on temperature and strain rate, grain refinement is the only strengthening mechanism which improves both strength and ductility simultaneously. Increasing the strength through grain refining is best described by the Hall–Petch relationship which assumes an inverse correlation between flow stress and grain size. FCC and BCC materials, which mainly deform through dislocation slip, show significant increase in their strength with a reduction in grain size induced by the ECAP process, although the strain hardening capacity might decline depending on microstructural features and the processing temperature [7–10]. However, the flow stress in magnesium alloys does not respond to grain refinement according to the classical Hall–Petch relationship if the effects of texture components on deformation mechanisms are not considered [11–18]. In other words, a decrease in grain size does not necessarily result in an increase of yield stress if the loading is not carried out with respect to a constant texture component. Yield stress in tension and shear of extruded magnesium decreases after ECAP [19–24]. In contrast, compressive yield stress shows an increasing trend with number of ECAP cycles [21].

The importance of texture in plasticity of wrought magnesium stems from the remarkable contribution of twinning to the plastic deformation of magnesium alloys [25,26]. The twin system most frequently observed in magnesium is $\{1\bar{1}02\}\langle 1\bar{1}00\rangle$[27]. This mode of twinning occurs when internal stresses create a tensile stress along the c-axis of the crystal. Therefore, unlike dislocation slips which can take place on two exactly opposite loading directions

* Corresponding author.
E-mail address: farhoud1@umbc.edu (F. Kabirian).

http://dx.doi.org/10.1016/j.jallcom.2016.02.145
0925-8388/

(e.g. tensile and compression along one specific direction), twins form only under one strain path, i.e. twinning does not occur in the opposite path [27,28]. This underlines the effect of the loading direction with respect to the texture components in the occurrence of twinning in magnesium alloys. In this regard, several studies focused on the calculation of Schmid factors (SF) for twinning in magnesium alloys and the resultant texture [29–31] under various loading directions.

The polar nature of twinning initiates the complexities associated with magnesium alloys' mechanical properties such as yield asymmetry and mechanical anisotropy. Presence of a stronger texture results in a more pronounced yield asymmetry and mechanical anisotropy. In magnesium with texture the propensity to twinning deformation depends on grain size, temperature, and strain rate [32–35]. Wang et al. [32] showed that there is a distinct correlation between the number fraction of twinned grains and grain size. According to this study, the twin fraction is larger for coarse grained magnesium alloys. It was also shown that since the twinning formation is less probable at smaller grain size a reduced tension-compression yield asymmetry is expected [21,32]. Thus, under the same loading condition, activities of deformation mechanisms in magnesium alloys with similar texture but different grain size are expected to be different.

To date, many studies have investigated the effect of ECAP on mechanical properties and texture evolution of magnesium alloys specifically under tensile loading, however, there is still a limited discussion on these aspects under a wide range of temperature and strain rate, in particular, in compressive loading. This could be of great importance due to the notable mechanical anisotropy in compression depending on the orientation of loading direction with respect to c-axis [35]. In general, ductile metals can accommodate plastic deformation in compression without failure, however, non-ductile materials like magnesium alloys fracture catastrophically on their shear plane leading to complete disintegration. Applications such as extrusion and rolling that involve compressive loadings require the knowledge of plastic flow at large strains, and the measurement of flow behavior using compressive testing is necessary. The present work focuses on mechanical properties and texture evolution of ECAPed magnesium at a wide range of temperature and strain rate under compression in different directions. Utilizing the Visco-Plastic Self Consistent (VPSC) modeling, the contribution of possible deformation mechanisms in compressive deformation is also studied.

2. Materials and experimental procedures

Commercial AZ31B magnesium alloy was received in extruded form. Neutron diffraction texture measurements were conducted for the as-received and ECAPed materials and also deformed samples. Using the MTEX algorithm developed by Hielscher and Schaeben [36], the orientation distribution function (ODF) was calculated.

The compression cylinders (5 mm in diameter and 7 mm in length) were machined from the as-received magnesium parallel and perpendicular to the extrusion direction designated as ED and PED, respectively (Fig. 1a). The chosen dimensional ratio for samples, i.e. L(height)/D(diameter) = 1.4, provides the lowest friction between sample and compression anvil while buckling is avoided. These specimens were cut in equal radial distances from the center of extruded rod to factor out the effects of possible non-homogeneity in texture and grain structure throughout the material's cross section.

The ECAP billets had the dimensions of 12.7 mm × 12.7 mm × 82.5 mm. The ECAP die had a channel angle of 90° and a corner angle of 20°. For these dimensions, the equivalent strain for each pass subjected to each specimen is about 1. Tungsten disulfide (WS_2) grease was used as a lubricant. The die was preheated to 523 K. The billets were pressed at a speed of 1 mm/s and using route B_C (90° rotation of the billet in the same direction after each pass). After the billets were pressed for the final time they were assigned a billet coordinate system based on the pressing direction on the final product. The x, y and z directions are labeled in Fig. 1b in where, y is aligned with the pressing direction (PD) and x and z are perpendicular and transverse to the pressing directions (ND and TD). Note that ND and TD have a certain orientation with respect to the shear direction.

Room temperature quasi-static compression specimens had been pressed for two and four passes. The cylindrical specimens, 5 mm in diameter and 7 mm in length, were machined from the billets parallel to PD, ND, and TD. An MTS axial/torsion servo-hydraulic 809 system, with an axial load capacity of 250 kN equipped with an interface load cell of 25 kN, was used to perform all of the quasi-static experiments. Experiments performed on specimens were at strain rates of 10^{-4}, 10^{-2} and 10^{0} s^{-1}. To study the material response over a wide range of temperatures, the same engineering strain rates given before were conducted at temperatures of 77 K (liquid nitrogen, LN2) and 423 K for the ECAPed material. To reduce the effect of friction on the uniformity of deformation and maintaining uniaxial stress state and also to avoid barreling during the compression experiment, the interface between the specimen and MTS fixture platens was lubricated with a combination of Teflon sheet of 0.076 mm in thickness and high vacuum grease at room temperature. High temperature tungsten disulfide (WS_2) grease was used as a lubricant in case of compression experiments at high temperatures.

The split-Hopkinson pressure bar technique (SHPB) was utilized to perform dynamic uniaxial compression experiments on samples that were subjected to four passes of ECAP, at an engineering strain rate of about 3000 s^{-1}. In this study, the pressure bars were made out of 12.7 mm diameter Vascomax C350 maraging steel. The high strain rate cylindrical specimens were 6.6 mm in diameter and 3.5 mm in length. An annealed copper C110 "pulse shaper" of 6.35 mm in diameter and 0.25 mm thickness was used to dampen the undesirable oscillations and noise from the test. The same temperatures given before were performed. To monitor the texture evolution during dynamic compression experiment, some loadings were interrupted at selected intermediate strains. This task was accomplished by placing a ring with a specific thickness between the incident and transmitted bars while the sample was in the center of the ring. To impose different strains, spacers with different thicknesses of 3.278 ± 0.001 mm and 3.165 ± 0.001 mm were placed between incident and transmitted bars.

3. Results and discussion

3.1. Microstructural and texture evolution after ECAP

The evolution of grain-structure and texture after two and four passes of ECAP are shown in Fig. 2. Even though a remarkable reduction in grain size after two passes of ECAP is observed, a non-uniform grain structure prevails. Increasing the number of passes to four reduces the non-uniformity in grain size distribution and also slightly reduces the average grain size. The average grain size of ~13 μm in extruded AZ31reduces to 6.8 μm and 5.2 μm after two and four passes of ECAP, respectively. Similar observations in grain size changes with the number of ECAP passes has been observed in a study conducted by Dumitru et al. [37] on effects of ECAP on ZK60 magnesium alloy.

Crystal orientation also experiences remarkable changes after ECAP. While the basal poles in the extruded condition are

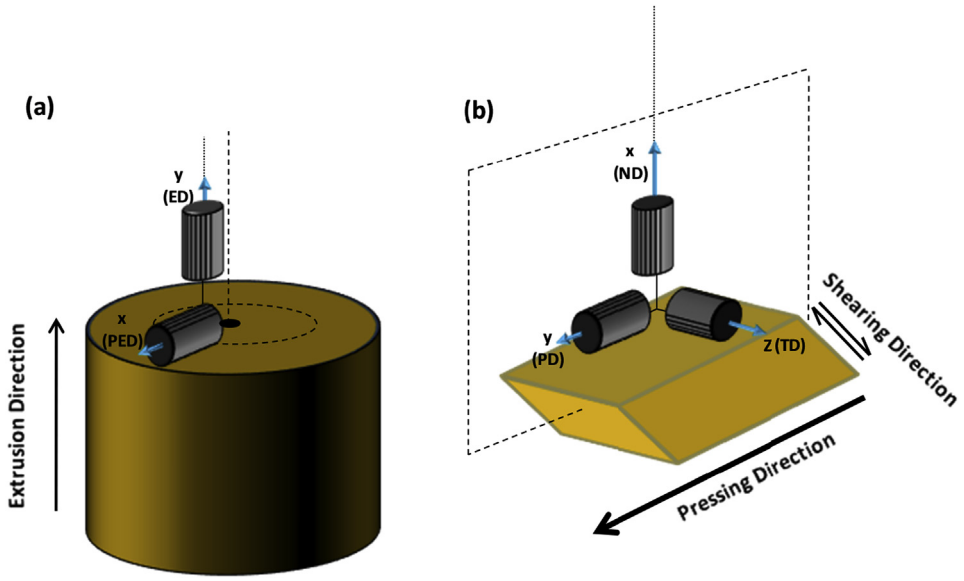

Fig. 1. Orientations of compression samples machined from a) extruded and b) ECAPed billets. Note to the orientations of ND and TD samples with respect to the shear direction.

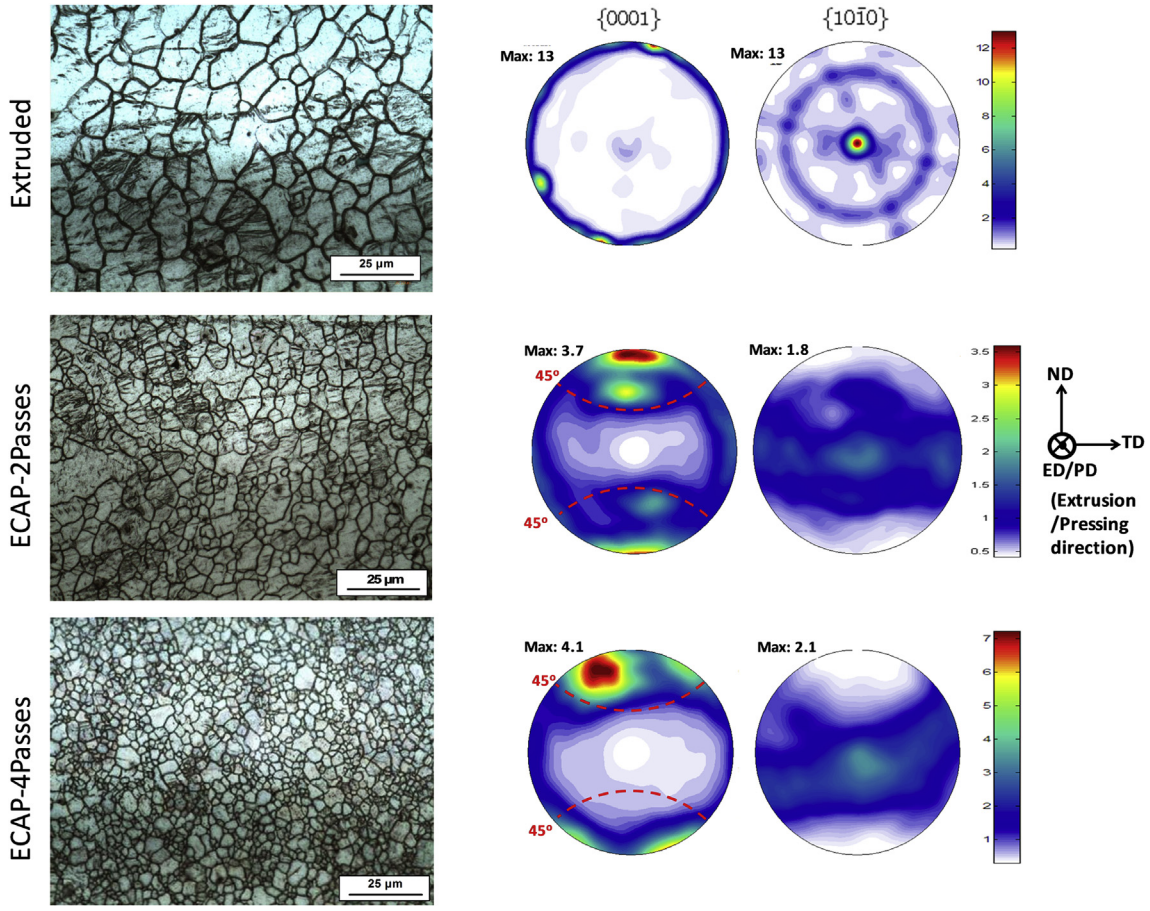

Fig. 2. Optical microscopy and measured pole figures of as-extruded and ECAPed AZ31 after two and four passes.

distributed axi-symmetrically perpendicular to the extrusion direction, after two passes of ECAP (2P-ECAPed), the majority of basal poles reorients toward ND. By increasing the number of passes to four (4P-ECAPed), basal planes are more inclined to be aligned with the shear plane during ECAP (Fig. 1b), thus basal poles in 4P-ECAPed are oriented between ND and 45° with respect to the pressing direction. Texture evolution depends on the ECAP route and pressing temperature [38–40]. Agnew et al. [38,39] showed that increasing

the number of ECAP-B_c results in development of a stronger texture. The texture measured by Mostaed et al. [40] reveals that decreasing the pressing temperature during route B_c leads to a stronger texture such that most of the basal planes are aligned with shear plane during the ECAP.

3.2. Mechanical experiments results

Mechanical responses after compressive loading in ED and PD for extruded AZ31and ECAPed magnesium, respectively, are shown in Fig. 3. The yield strength of the extruded material is slightly lower than 100 MPa and the stress–strain curve shows characteristics of twinning-dominated plastic deformation, i.e., there is a maximum in strain hardening rate at some intermediate strain. The ECAPed samples show a substantial increase in yield strength. However, when the number of ECAP passes increases from two to four a slight decrease in yield strength is observed. Despite the higher yield strength of the ECAPed material in comparison to the as-extruded condition, strain-hardening rate is significantly lower along the processing direction and it decreases more with increasing the number of ECAP passes. These observations will be explained in more details considering the starting texture in Sec. 3.3.

The observed mechanical responses are a result of grain size and initial texture through their effects on deformation mechanisms. In order to understand the roles of possible deformation mechanisms, the VPSC simulation was utilized [41]. The relative activities of the different deformation mechanisms which is the relative contribution of each deformation mode and the average number of active system per grain were obtained after the VPSC model was calibrated to the best fit of both the stress–strain curves and the texture simulation (Fig. 4). Details of the VPSC modeling can be found elsewhere [35]. Plastic yielding in extruded AZ31 is dominated by twinning. Twinning activity dwindles with strain while that for basal slip increases gradually so that at the intermediate strain of 6.5%, deformation is dominated by basal slip. Throughout the whole deformation of the extruded sample, activities of prismatic and pyramidal slips stay below 10%.

Texture evolution alongside the grain refinement induced by ECAP results in remarkable changes in the relative activity of deformation mechanisms when loading is performed parallel to the PD. Plastic yielding in the ECAPed samples is dominated by basal slip, however, twinning is still playing a major role in accommodation of plastic deformation. Since the activity of twinning is higher in extruded AZ31, a larger volume of hard orientation for the following basal slip is expected. Hence, the resulted strain hardening is significantly higher in the as-extruded condition compared with ECAPed AZ31. On the other hand, non-basal slip mechanisms show more activity in the ECAPed samples so that after four passes prismatic and pyramidal slips precede twinning at an earlier stage of deformation. This facilitates accommodation of plastic deformation especially along the c-axis resulting in lower strain hardening and higher fracture strain in ECAPed magnesium. As it is shown in Fig. 3, not only the fracture strain increases with ECAP passes but s-shape strain-hardening reduces due to the higher contribution of pyramidal <c + a> slip in compliance with deformation along the c-axis.

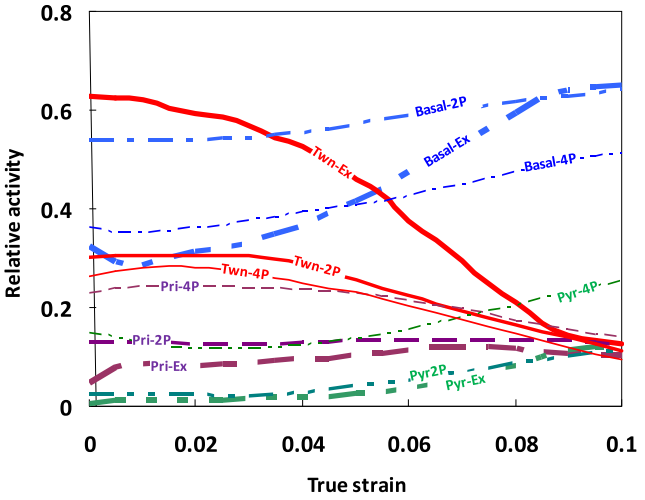

Fig. 4. Relative activity of different deformation mechanisms versus compressive plastic strain predicted by VPSC in both extruded and ECAPed materials along ED/PD.

Due to the presence of axi-symmetric texture in extruded AZ31 the strain hardening response is the same in all perpendicular directions. However, a mechanical anisotropy in ECAPed AZ31prevails when loading is carried out perpendicular to the pressing direction (Fig. 5). A pronounced s-shape strain hardening response is observed during loading in the TD of ECAPed AZ31 (Fig. 5). This response is more appreciable in the 2P-ECAPed sample resulting in

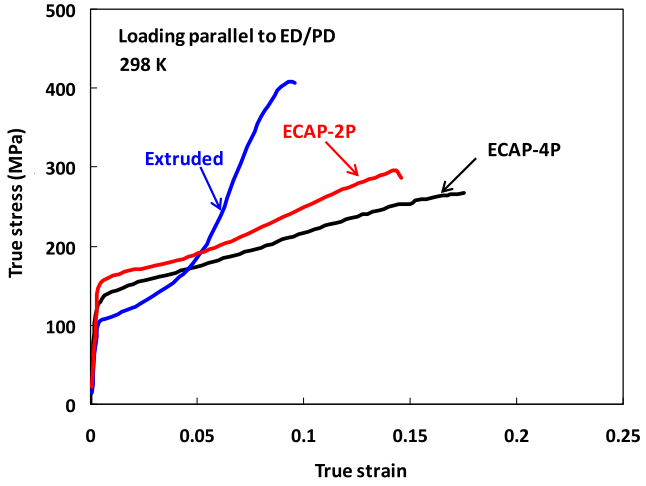

Fig. 3. Mechanical responses of as-extruded and ECAPed AZ31 parallel to the extrusion/pressing direction.

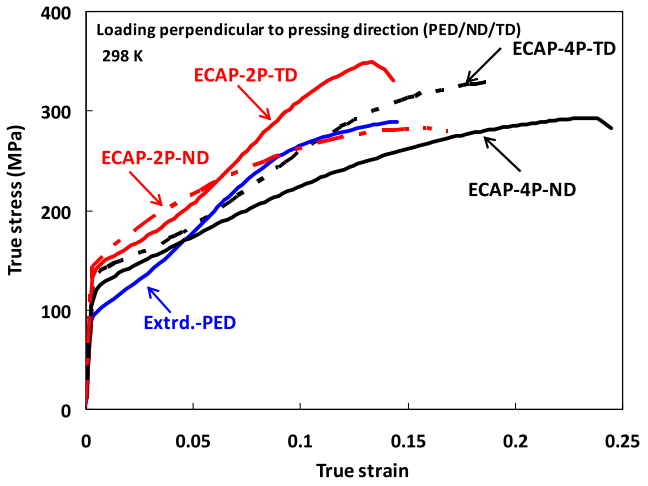

Fig. 5. Mechanical responses of as-extruded and ECAPed AZ31 perpendicular to the ED/PD.

a higher flow stress compared with the 4P-ECAPed sample. Contrary to the TD sample the s-shape strain hardening response in the ND of ECAPed AZ31is significantly reduced so that strain hardening behavior in the ND of 2P-ECAPed sample resembles the typical power shape response.

In order to examine effects of strain rate and temperature on mechanical responses of fine grained AZ31, the 4P-ECAPed AZ31 was subjected to compressive loading in the PD and TD at the temperature range of 77–423 K under the strain rate of 10^{-4}–3000 s^{-1} (Fig. 6). Loading in both directions at 77and 298 K, is not associated with a marked change in mechanical responses when strain rate changes from 10^{-4}–10^{0} s^{-1}. In contrast, increasing the strain rate to 3000 s^{-1} raises strain-hardening rate over the same temperature range. Furthermore, the concavity of stress–-strain curve, in particular in the PD, is reduced during loading under the high strain rate (3000 s^{-1}) deformation. In addition, occurrence of maximum strain hardening rate shifts to the lower strains. These described characteristics are at maximum intensity during the cryogenic loading at 3000 s^{-1}. As it is observed, the material toughness increases drastically under this loading condition. More information about effects of cryogenic temperatures on ductility and toughness can be found in Refs. [42,43].

The negligible difference in the mechanical behavior between 10^{-4} and 10^{0} s^{-1} becomes pronounced when temperature is increased to 423 K. Even though room temperature stress–strain curves in the PD and TD feature s-shape strain hardening, decreasing the strain rate to 10^{-4} s^{-1} at 423 K does not show this characteristic. Twinning-induced plastic deformation is featured by the s-shape strain hardening curve, however, absence of this characteristic is not necessarily indication of suppression of twinning and considerations of texture evolution should be taken into account. The significant mechanical anisotropy observed at room temperature or even at high temperature under high strain rates is diminished during the deformation at 423 K under the strain rate of 10^{-4} s^{-1}.

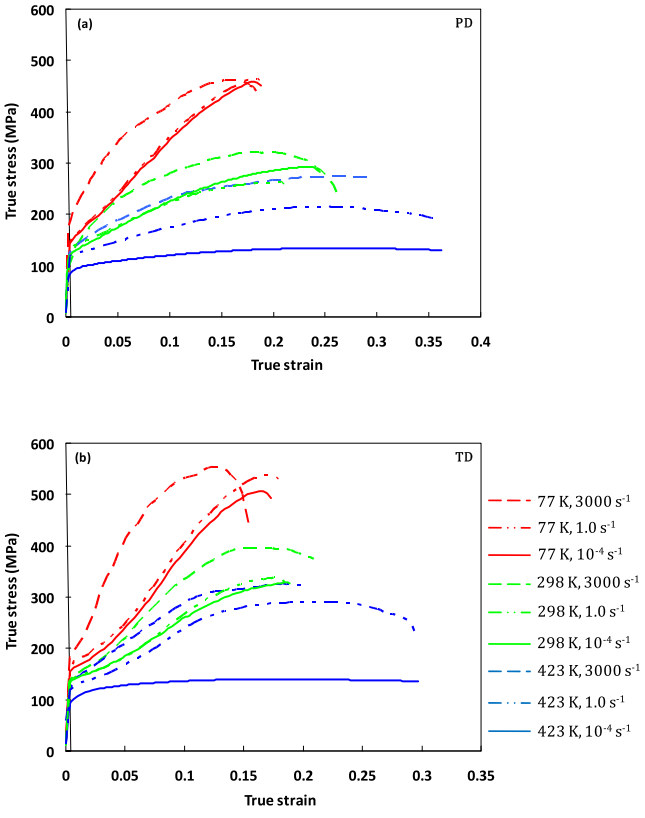

Fig. 6. Compression stress–strain curves of 4P-ECAPed AZ31 at different temperatures and strain rates in the (a) PD and (b) TD.

Strain rate and temperature sensitivity of the ECAPed material in different directions can be better depicted in Fig.7. Variations in yield strength and maximum stress at investigated temperatures and strain rates are shown in this figure. There is no appreciable change in both yield stress and maximum stress in the PD and TD with changes in strain rate at low temperatures. However, with increasing the temperature to 423 K both yield stress and maximum stress show a noticeable dependency on strain rate. The increase in flow stress with strain rate is more pronounced over the 10^{-4}–10^{-2} s^{-1} range.

3.3. Texture evolution

Fig.8 shows the loading direction inverse pole figure for extruded and 4P-ECAPed AZ31at plastic strain of 0.055 in compression along the PD. It is evident that both materials have undergone crystal reorientation, though in different fashions. The majority of grain volume has twinned in extruded AZ31 (dashed versus solid rectangles in Fig. 8a), i.e. crystal reorientation due to twinning in extruded AZ31 is a sudden change such that two modes of crystal orientation are distinguished; a small volume of grains which still preserve the initial orientation (solid rectangle) and the majority of grains which have already twinned (dashed rectangle). The twinned grains have their basal planes {0001} almost normal to the loading direction. On the other hand, crystal reorientation due to twinning takes place at a much slower rate in 4P-ECAPed AZ31 (Fig. 8b) so that at the same level of plastic strain (~0.055), a more uniform distribution of crystallographic planes with respect to the loading direction is observed. The dominant texture component in this condition is$\{\bullet\bar{2}\bullet 3\}$.

SF maps calculated for $(1\bar{1}02)[\bar{1}101]$ twin variants and basal <a> slip explain the difference in crystal reorientation due to twinning in the extruded and ECAPed materials. The calculation of SF for the hexagonal crystal structure is more complicated and less straightforward than cubic materials [29,30]. The method used for calculation of SF in this study has been explained in more details in Ref. [44]. Here, we only present the final form of the equation for compressive loadings:

$$m = -\frac{u_1u_2 + v_1v_2 + t_1t_2 + \lambda^2 w_1w_2}{\left(u_1^2 + v_1^2 + t_1^2 + \lambda^2 w_1^2\right)^{0.5}\left(u_2^2 + v_2^2 + t_2^2 + \lambda^2 w_2^2\right)^{0.5}} \times \frac{h_1u_2 + k_1v_2 + i_1t_2 + l_1w_2}{\left(h_1^2 + k_1^2 + i_1^2 + \lambda^{-2} l_1^2\right)^{0.5}\left(u_2^2 + v_2^2 + t_2^2 + \lambda^2 w_2^2\right)^{0.5}} \quad (1)$$

The first and second terms in this expression are the cosine of the angle between the slip direction $[u_1v_1t_1w_1]$ and the loading axis $[u_2v_2t_2w_2]$ and cosine of the angle between normal to slip plane$[h_1k_1i_1l_1]$ and the loading axis$[u_2v_2t_2w_2]$, respectively. Also, $\lambda^2 = 2/3\left(c/a\right)^2$. The negative sign is representative of compressive loadings. In case of tension loading, the negative sign will be replaced by a positive.

In general, the SF varies in the range of −0.5 to 0.5. A change in the sign of SF implies a change in the direction of the resolved shear stress on the slip plane along the slip direction. As it was mentioned before, due to the polar nature of twinning, if a shear direction favors occurrence of twinning, shear in the opposite direction does not result in twin formation. For example, in this study only loading directions associated with positive SF values are able to activate extension twinning. In the SF map shown in Fig.9 only constant SF

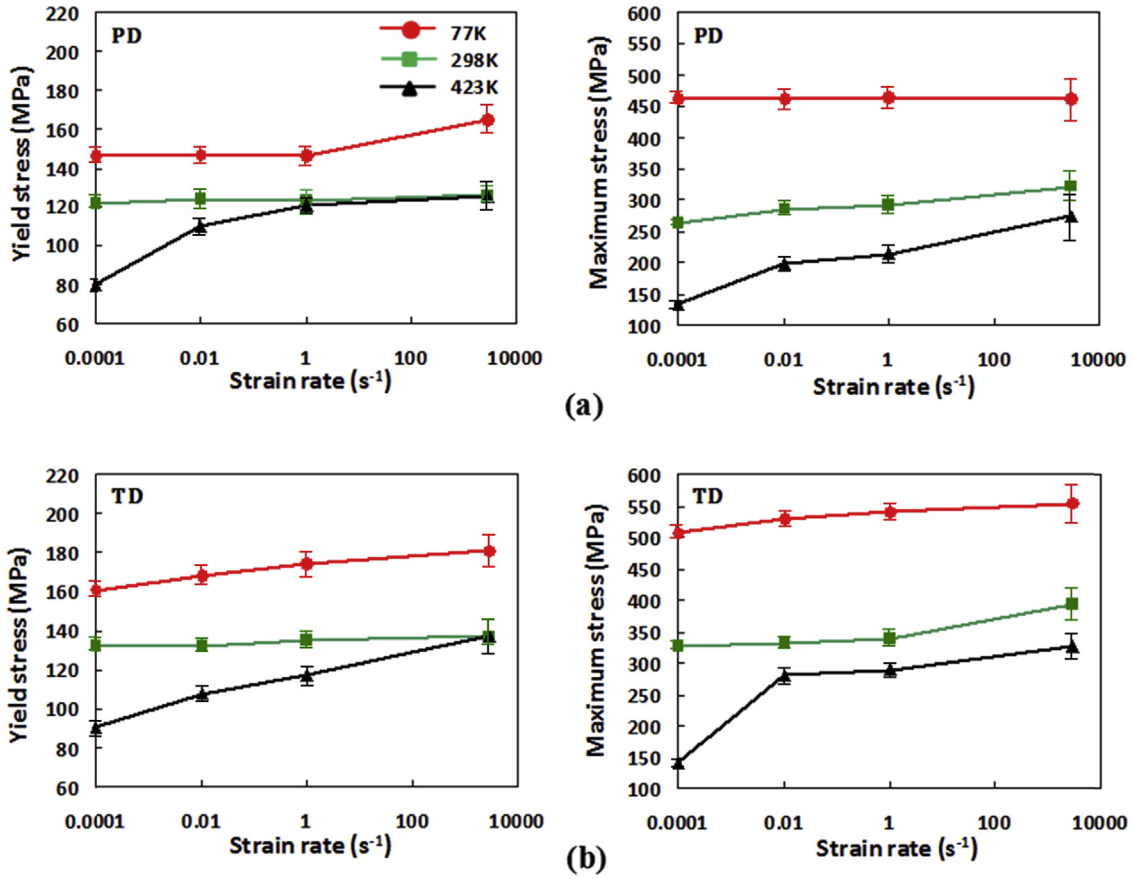

Fig. 7. Variations of yield stress and maximum stress with strain rates at different temperatures for 4P-ECAPed AZ31 in (a) PD and (b) TD. Standard deviation is based on three different measurements.

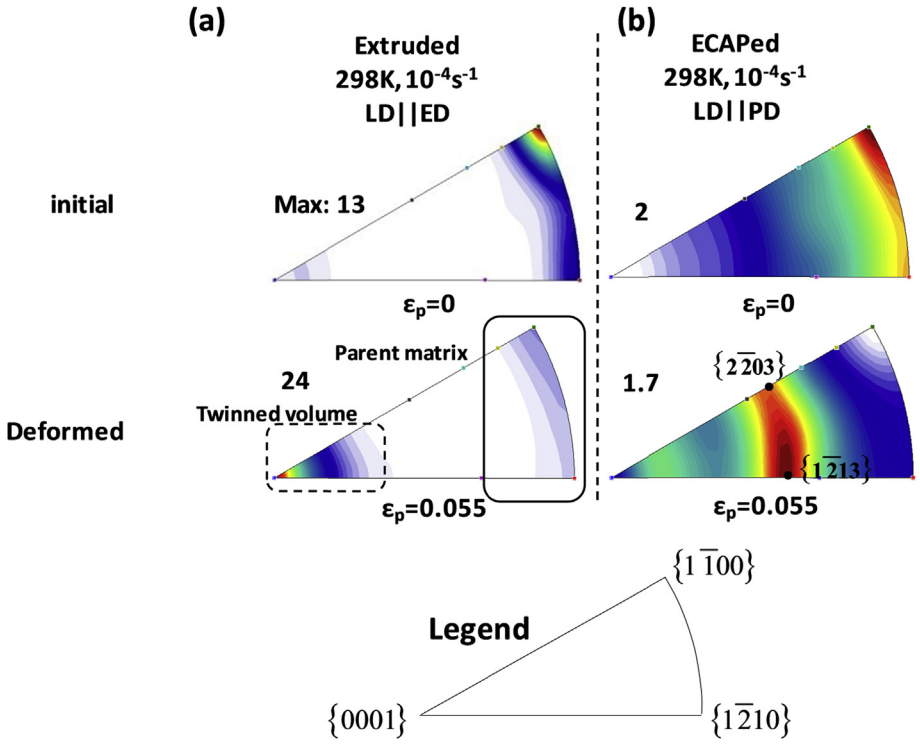

Fig. 8. Loading direction inverse pole figures showing texture evolution after 0.055 compressive strain in (a) extruded AZ31 along the ED and (b) 4P-ECAPed AZ31 along the PD.

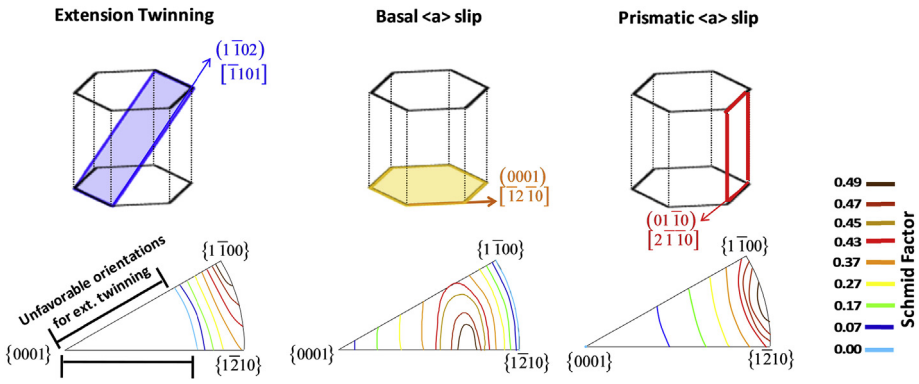

Fig. 9. Calculated Schmid Factor maps for both twinning and basal <a> slip. Shear planes and directions are highlighted. Note that the calculated maps are based on slip or twin variants with the maximum SF.

contours resulting in the activation of extension twinning (positive SF values) under uniaxial compression are shown. Comparing the SF maps for the different mechanisms shows that loading directions with high SF for twinning are less capable of creating deformation through basal <a> slip considering the latter has its minimum SFs overlapped with these directions. As it is observed, unlike extruded magnesium in which the majority of grains are in orientations with high SF values for twinning, in the ECAPed material only a small fraction of grains offer the favorable orientation for twinning. Therefore, in the ECAPed material, only grains with high SF values have been reoriented due to twinning resulting in increased density of grains with{0001} planes normal to the loading direction. On the other hand, according to the obtained SF map for basal <a> and prismatic <a> slips, there are more chances for these mechanisms to accommodate plastic deformation in the ECAPed material compared with the extruded one since there is a higher concentration of grains with high SF values. These results are in agreement with the VPSC simulation (Fig. 4) where the reduced activity of twinning in comparison to basal <a> slip is predicted in the ECAPed material.

Loading in the extreme condition, i.e. high temperature dynamic loading does not affect the twinning response in extruded AZ31 (Fig. 10a). For a smaller plastic strain (~0.035), the extruded material still shows two distinct orientations of parent matrix and twinned volume. Also, ECAPed magnesium still shows the gradual reorientation of crystals with plastic strain, however, there is some evidence of twinned grains marked by the dashed circle in Fig. 10b. Even though increasing the temperature accelerates dislocation recovery and, in turn, allows more deformation to be accommodated by slip mechanisms, the high rate of deformation at 3000 s^{-1} precedes the kinetic of the recovery process. Hence, this allows for more possibilities to twinning to contribute to deformation in contrast to quasi-static loading. On the other hand, decreasing the strain rate to 10^{-4} s^{-1} provides enough time for dislocation recovery and thus, higher capacity for slip mechanisms to accommodate plastic deformation. In spite of this fact, twinning in extruded AZ31plays a major role in deformation at high temperature slow rate loading (Fig. 10c). As it is shown in Fig. 10c, significant crystal reorientation in the extruded material under high temperature slow rate loading is still detected, however, its intensity and extent is noticeably lower than that at room temperature (Fig. 10c). Measured texture of ECAPed material under high temperature slow rate deformation (423 K-10^{-4} s^{-1}) still suggests occurrence of twinning (Fig. 10d). On the other hand, the obtained stress–strain curve under this loading condition does not show the typical characteristic of twinning-dominated plastic deformation which is the s-shape hardening (Fig. 6). As mentioned before, the SF maps (Fig. 9) predict the higher activity of twinning and prismatic slip than basal slip in the ECAPed material as the crystal orientation is more favorable for these mechanisms. However, due to high level of critical resolved shear stress (CRSS) associated with prismatic slip, this mechanism is less active at room temperature and thus, plastic deformation is mainly accommodated by basal slip and twinning. On the other hand, with increasing temperature, the associated CRSS for prismatic slip decreases and gives a rise to activity of this mechanism at high temperature. Increased activity of slip

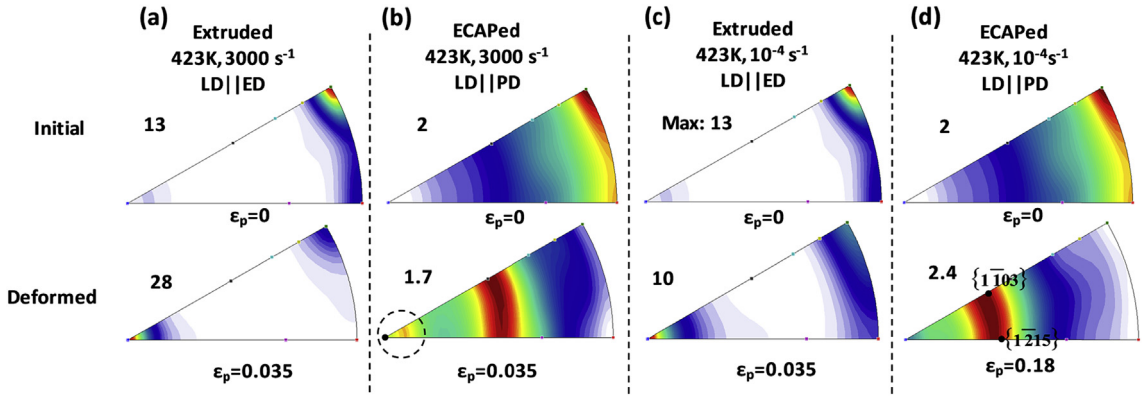

Fig. 10. Loading direction inverse pole figures showing texture evolution after some compressive strain in (a,c) extruded and (b,d) ECAPed materials at high temperature and different strain rates. The dashed circle indicates the occurrence of twins.

mechanisms, in particular non-basal slip, together with higher rate of dislocation recovery with respect to deformation rate (10^{-4} s^{-1}) result in the typical power shape strain hardening under loading at 423 K and 10^{-4} s^{-1} even though twinning is still active. Compared to the high strain rate deformation, the dominant texture under this condition (423 K – 10^{-4} s^{-1}), is more shifted to the planes parallel to basal planes. This shift in maximum intensity could be result of rotation of crystals due to the slip of dislocation or profuse grain-boundary sliding at high temperature.

Texture evolution during loading in the direction perpendicular to the extrusion/pressing direction in both extruded and ECAPed AZ31 were also studied. Loading along ND in the ECAPed material might not be associated with twin formation as almost all of the grains in this direction present negative SF values which is the unfavorable orientation for twinning (Fig. 11). Loading in TD subjects a higher portion of grains with positive SF to extension twinning, although the grains in the latter case are not necessarily oriented towards the maximum SF. This clarifies why the stress–strain curve in ND (Fig.5) almost presents a typical power curve while loading in TD is associated with an s-shape strain hardening. Texture evolution during high temperature dynamic loading in TD reveals the same characteristics (Fig. 11), i.e. crystal reorientation due to twinning, however, with a stronger texture compared to quasi-static deformation at room temperature. It should be mentioned that this study only took the effects texture and crystal reorientation on plastic deformation. A conclusive discussion on roles of different deformation mechanisms on plasticity can be made when effects of dislocation structure and density are taken into account that requires more sophisticated characterization methods [45].

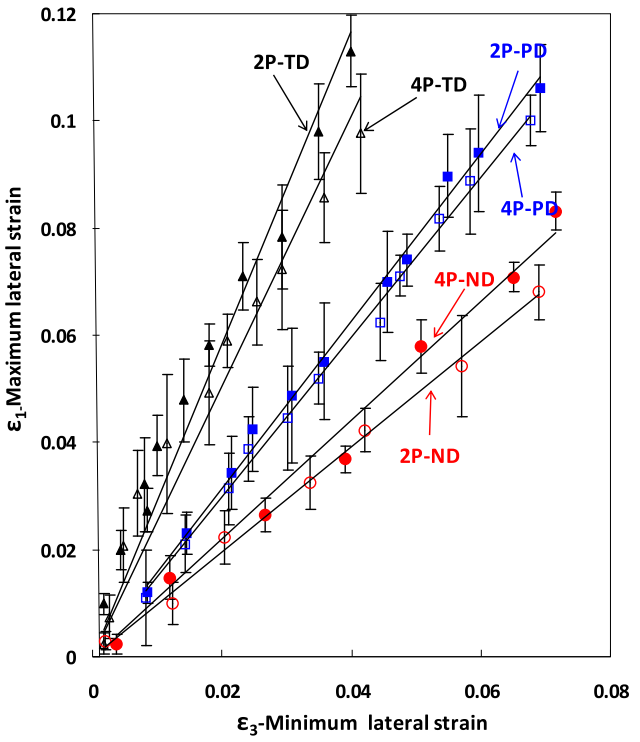

Fig. 12. Measured lateral strains for the ECAPed material at different directions. The uncertainty of measurements is "one sigma".

3.4. Biaxial anisotropy

Biaxial anisotropy as the ratio of maximum lateral strain to the minimum value was also investigated in the ECAPed material. An oval cross section is indicative of anisotropy in plastic deformation. In other words, an isotropic material would maintain its circular cross section during deformation assuming ideal lubrication [46]. During the compression loading, test was interrupted at specific intermediate strains and measurements in transverse directions were carried out. Variations of maximum lateral strain versus minimum lateral strain for the ECAPed samples in different loading directions are shown in Fig.12. In case of an isotropic material, the slope of this curve should be close to unity. The maximum anisotropy is observed when the loading direction is perpendicular to the pressing direction, i.e., TD. In case of loading in ND, there is almost no biaxial anisotropy as the slope of the curve is close to one and the curve for loading in PD lies between these two conditions. The difference in anisotropic behavior is the result of different deformation mechanisms in different directions. For example, the TD sample has the most favorable crystal orientations for the occurrence of twinning. However, the distribution of grain orientations with respect to the loading direction is not axi-symmetric, and a large degree of non-uniformity in lateral deformation is expected.

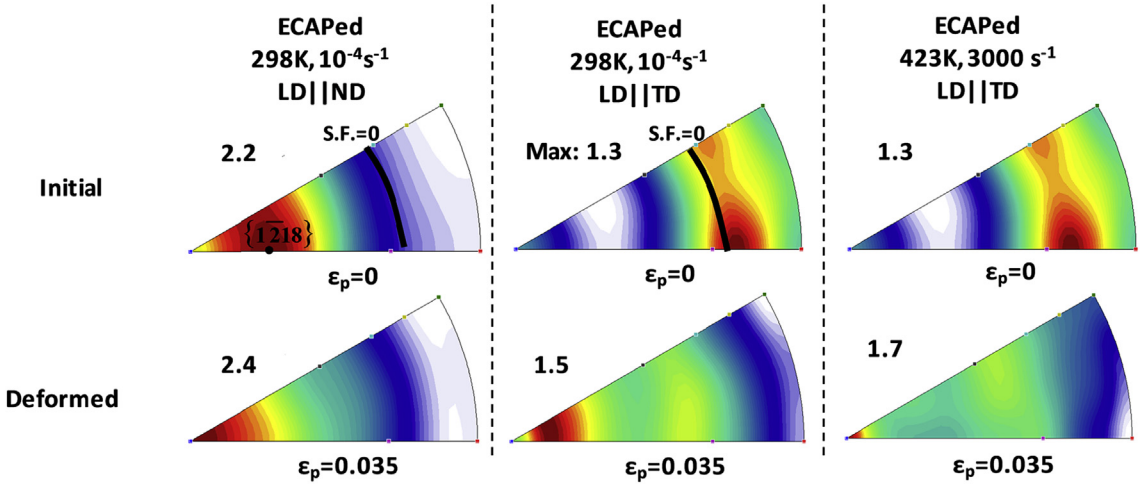

Fig. 11. Loading direction inverse pole figures showing texture evolution after some compressive strain in the perpendicular directions for the 4P-ECAPed material. Note that the black line represents the SF = 0 orientations.

Anisotropic deformation is more pronounced in the 2P-ECAPed sample since grain orientations are more favorable for occurrence of twinning. Unlike the TD sample the ND sample does not exhibit substantial twinning due to the large fractions of grains with their c-axis almost parallel to the loading direction especially in the case of the 2P-ECAPed sample. In this case, non basal<c + a> slip mechanisms control the plastic deformation and since the crystals orientation is symmetric with respect to the loading direction lateral deformation occurs uniformly.

4. Conclusions

Mechanical responses and texture evolution of the ECAPed AZ31 magnesium alloy under a wide range of temperature (77 K–423 K) and strain rate (10^{-4} s^{-1}–3000 s^{-1}) were studied. Uniaxial compression experiment was conducted parallel and perpendicular to the pressing direction.

Calculated SF maps together with VPSC results were also employed to explain the difference in deformation behavior of extruded and ECAPed materials. Twinning deformation and basal slip were found as the dominant mechanisms in plastic yielding of extruded and ECAPed materials, respectively. Strain hardening response in ECAPed AZ31 shows a strong dependency on strain rate and temperature in both PD and ND. At the same strain rate, hardening due to twinning became more pronounced with decreasing the testing temperature to 77 K while a typical power shape strain hardening response at the highest temperature (423 K) and lowest strain rate (10^{-4} s^{-1}) was observed. Even though s-shape strain hardening was absent under the later loading condition, texture measurement still revealed crystal reorientation due to twinning implying that the absence is not necessarily indicative of suppression of twinning. In other words, due to higher activity of non-basal slip system at high temperatures in addition to the kinetic of dislocation-recovery rate with respect to strain rate, the significant strain hardening due to twinning does not occur anymore. In contrast, loading at a high strain rate (~3000 s^{-1}) resulted in occurrence of maximum strain hardening rate at smaller strains.

5. Disclaimer

Certain commercial firms and trade names are identified in this report in order to specify aspects of the experimental procedure adequately. Such identification is not intended to imply recommendation or endorsement by the National Institute of Standards and Technology, nor is it intended to imply that the materials or equipment identified are necessarily the best available for the purpose.

References

[1] A. Yamashita, Z. Horita, T.G. Langdon, Mat. Sci. Eng. A 300 (2001) 141–147.
[2] E. Mostaed, A. Fabrizi, D. Dellasega, F. Bononllo, M. Vedani, J. Alloys Comp. 638 (2015) 267–276.
[3] R.B. Figueiredo, T.G. Langdon, J. Mat. Sci.. (43) 7366–7371.
[4] F.M. Lu, A.B. Ma, J.H. Jiang, D.H. Yang, Y.C. Yuan, L.Y. Zhang, J. Alloys Comp. 601 (2014) 140–145.
[5] Y.C. Yuan, A.B. Ma, J.H. Jiang, Y. Sun, F.M. Lu, L.Y. Zhang, D. Song, J. Alloys Comp. 594 (2014) 182–188.
[6] Y. Miyahara, Z. Horita, T.G. Langdon, Mat. Sci. Eng. A 420 (2006) 240–244.
[7] E.A. El-Danaf, M.S. Soliman, A.A. Almajid, M.M. El-Rayes, Mat. Sci. Eng. A 458 (2007) 226–234.
[8] E.A. El-Danaf, Mat. Sci. Eng. A 189 (2008) 189–200.
[9] O.F. Higuera-Cobos, J.M. Cabrera, Mat. Sci. Eng. A 571 (2013) 103–114.
[10] H.W. Kim, S.B. Kang, N. Tsuji, Y. Minamino, Acta Mat. 53 (2005) 1737–1749.
[11] F. Akbaripanah, F. Fereshteh-Saniee, R. Mahmudi, H.K. Kim, Mat. Des. 43 (2013) 31–39.
[12] Y. He, Q. Pan, Y. Qin, X. Liu, W. Li, Y. Chiu, J.J.J. Chen, J. Alloys Comp. 492 (2010) 605–610.
[13] J.A. del Valle, F. Carren, O.A. Ruano, Acta Mat. 54 (2006) 4247–4259.
[14] H.K. Kim, Mat. Sci. Eng. A 515 (2009) 66–70.
[15] W.M. Gan, M.Y. Zheng, H. Chang, X.J. Wang, X.G. Qiao, K. Wu, B. Schwebke, H.G. Brokmeier, J. Alloys Comp. 470 (2009) 256–262.
[16] W.J. Kim, C.W. An, Y.S. Kim, S.I. Hong, Acta Mat. (2002) 4739–4744.
[17] Y. Wang, H. Choo, Acta Mat. 81 (2014) 83–97.
[18] B. Chen, D. Lin, X. Zeng, C. Lu, J. Alloys Compd. 440 (2007) 94–100.
[19] S.M. Masoudpanah, R. Mahmudi, Mat. Sci. Eng. A (2009) 52622–52630.
[20] S.M. Masoudpanah, R. Mahmudi, Mat. Des. 31 (2010) 3512–3517.
[21] R. Jahadi, M. Sedighi, M. Jahed, Mat. Sci. Eng. A 593 (2014) 178–184.
[22] S. Seipp, M.F.X. Wagner, K. Hockauf, I. Schneider, L.W. Meyer, M. Hockauf, Int. J. Plast. 35 (2012) 155–166.
[23] G.D. Fan, M.Y. Zheng, X.S. Hu, C. Xu, K. Wu, I.S. Golovin, Mat. Sci. Eng. A 556 (2012) 588–594.
[24] M. Karami, R. Mahmudi, Mat. Sci. Eng. A 607 (2014) 512–520.
[25] B. Beausir, S. Suwas, L.S. Toth, K.W. Neale, J.J. Fundenberger, Acta Mat. 56 (2008) 200–214.
[26] F. Lu, A. Ma, J. Jiang, J. Chen, D. Song, Y. Yuan, J. Chen, D. Yang, J. Alloys Compd. 643 (2015) 2833.
[27] M.H. Yoo, Met. Trans. A 12 (1981) 409–418.
[28] P.G. Partridge, Metall. Rev. 12 (1967) 169–194.
[29] S.G. Hong, S.H. Park, C.S. Lee, Acta Mat. 58 (2010) 5873–5885.
[30] X. Zhang, Y. Cheng, J. Alloys Compd. 622 (2015) 1105–1109.
[31] S.H. Park, S.-G. Hong, J.H. Lee, Y.-H. Huh, J. Alloys Compd. 646 (2015) 573–579.
[32] J.T. Wang, D.L. Yin, J.Q. Liu, J. Tao, Y.L. Su, X. Zhao, Acta Mat. 59 (2008) 63–66.
[33] A. Ghaderi, M.R. Barnett, Acta Mat. 59 (2011) 7824–7839.
[34] N.V. Dudamell, P. Hidalgo-Manrique, A. Chakkedath, Z. Chen, C.J. Boehlert, F. Gálvez, S. Yi, J. Bohlen, D. Letzig, M.T. Pérez-Prado, Mat. Sci. Eng. A 583 (2013) 220–231.
[35] F. Kabirian, A.S. Khan, T. Gnäupel-Herlod, Int. J. Plast. 68 (2015) 1–20.
[36] R. Hielscher, H. Schaeben, J. Appl. Cryst. 41 (2008) 1024–1037.
[37] F.-D. Dumitru, O.F. Higuera-Cobos, J.M. Cabrera, Mat. Sci. Eng. A 594 (2014) 32–39.
[38] S.R. Agnew, P. Mehrotra, T.M. Lillo, G.M. Stoica, P.K. Liaw, Acta Mat. 53 (2005) 3135–3146.
[39] S.R. Agnew, P. Mehrotra, T.M. Lillo, G.M. Stoica, P.K. Liaw, Mat. Sci. Eng. A 408 (2005) 72–78.
[40] E. Mostaed, M. Hashempour, A. Fabrizi, D. Dellasega, M. Bestetti, F. Bonollo, M. Vedani, J. Mech. Behav. Biomed. Mat. 37 (2014) 307–322.
[41] R.A. Lebensohn, C.N. Tome, Acta Mat. 41 (1993) 2611–2624.
[42] D. Zhemchuzhnikova, A. Mogucheva, R. Kaibyshev, Mat. Sci. Eng. A 565 (2013) 132–141.
[43] J. Yi, S.M. Seifi, W. Wang, J.J. Lewandowski, J. Mat. Sci. Tech. 30 (2014) 627–630.
[44] P.R. Okamoto, G. Thomas, Phys. Status Solidi (b) 25 (1968) 81–91.
[45] I. Ghamarian, Y. Liu, P. Samimi, P.C. Collins, Acta Mat. 79 (2014) 203–215.
[46] F. Barlat, J.C. Brema, J.W. Yoon, K. Chung, R.E. Dick, D.J. Lege, F. Pourboghrat, S.-H. Choi, E. Chu, Int. J. Plast. 19 (2003) 1297–1319.